Fingertip Pulse-Echo Ultrasound and Optoacoustic Dual-Modal and Dual Sensing Mechanisms Near-Distance Sensor for Ranging and Material Sensing in Robotic Grasping*

Cheng Fang, Di Wang, Dezhen Song, and Jun Zou

Abstract— **To improve robotic grasping, we are interested in developing a new non-contact fingertip-mounted sensor for near-distance ranging and material sensing. Here we report new progress in combining direct pulse-echo ultrasound and optoacoustic effects in sensor design to deal with optically and/or acoustically challenging targets (OACTs). Our dual-modal and dual sensing mechanisms (DMDSM) sensor design is enabled by a novel wideband ultrasound transmitter embedded inside a piezoelectric (lead zirconate titanate - PZT) ring transducer. The new DMDSM sensor is capable of differentiating a variety of OACTs. To verify our design, both distance ranging tests and material sensing tests have been conducted. The ranging tests show the sensor can perform both optoacoustic ranging (for light-absorbing materials) and pulse-echo ultrasound ranging (for reflective or transparent materials). For material sensing, the dual-modal spectra from OACTs are collected to compare the new sensor with previous designs. The overall 100% accuracy from the confusion matrices indicates the initial success of our sensor design in differentiating conventional targets as well as the OACTs with the new DMDSM sensor.**

I. Introduction and Related Work

One of the grand challenges in robotics is the robust grasping of unknown objects [1] [2]. This is particularly important when robots expand its territory from industry floors to a wide range of domestic service applications where the prior knowledge of targeted objects is often not available. Sensor-less grasping has been well studied [3] [4]. However, it suffers from efficiency issues. Sensor-based approaches still dominate grasping operations. More specifically, object relative pose and material type/structure information are important for a successful grasp. Ideally, with the assistance of near-distance (e.g. < 0.5 cm) ranging, robotic fingers can respond to subtle changes in object pose right before the planned contact and adjust grasp operations dynamically. Moreover, the material-type and object internal structure information can help planner better estimate the force distribution, impact characteristics and friction coefficients for a more robust grasping.

Unfortunately, current sensors have difficulties in satisfying all these requirements despite significant progress made in recent development. Common sensors such as cameras, laser range finders, or radars all suffer from the occlusion caused by closing-in robot fingers in grasping [5] or having a near-range blind zone [6] [7] [8] [9]. Tactile sensing [10] [11] and force sensing [12] are also popular approaches. However, they require the robot to touch the object for sensing which may change object poses, damage the object, or lead to either slow grasping process or complete failure in grasping. A non-contact solution is more desirable.

Recent development of proximity/pre-touch sensors based on optical, electric-field, and ultrasound signals have achieved great progress. However, they still cannot satisfy the grasping requirements. Electric-field sensors have difficulties in detecting targets whose dielectric constants are close to that of air [13] [14] [15] [16]. The optical sensors lack the lateral resolution and are not effective for optically-transparent or highly-reflective targets [17] [18] [19] [20]. Existing ultrasound-based sensors, including seashell effect ones, fail on perceiving certain types of material, such as light object or sound absorbing materials [21] [22] [23] [24].

Previously, we have demonstrated finger-mounted non-contact sensors for near-distance ranging and material/thickness sensing using two different modalities: ultrasound and laser. The sensor designs are based on two sensing mechanisms: direct pulse-echo ultrasound and optoacoustic effects [25] [26] (Fig. 1). We name this design as a dual-modal and dual sensing mechanisms (DMDSM) design. The pulse-echo ultrasound utilizes ultrasound signals generated by a transducer to interrogate the distance and material properties of the target. In contrast, the optoacoustics relies on the direct generation of optoacoustic signals on the target with focused laser pulses. In both modalities, the sensor-object distance is estimated from the propagating delays of the acoustic signals. Their frequency spectra are used to extract distinctive features about the material and structure of the targets for classification. However, each sensing principle has its own limitations. For example, pulse-echo ultrasound could fail on targets (made of thin or porous materials) that have weak acoustic reflection or scattering. Optoacoustics would lose its effectiveness on targets that are either optically transparent or highly reflective, resulting in low optical absorption. We name them as optically and/or acoustically challenging targets (OACTs).

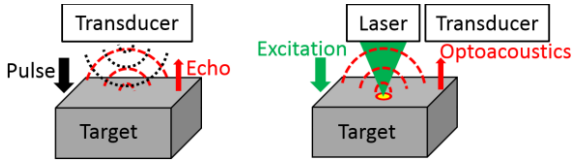

(a) (b)

*The research is supported in part by National Science Foundation under NRI-1925037.

C. Fang and J. Zou are with the Electrical and Computer Engineering Department, Texas A&M University, College Station, TX 77843, USA (e-mails: {fangchengok2007, junzou}@tamu.edu).

D. Wang and D. Song are with the Computer Science and Engineering Department, Texas A&M University, College Station, TX 77843, USA (e-mails: ivanwang@tamu.edu, dzsong@cs.tamu.edu).

Figure 1. Simplified diagrams of the two modalities and sensing mechanisms: (a) pulse-echo ultrasound, (b) laser and induced optoacoustics.

Therefore, to cope with the challenge brought by OACTs, a new combined design that simultaneously utilizes both pulse-echo ultrasound and optoacoustic effects for distance ranging and material sensing is desirable. However, due to the challenges and limitations in the sensor design, construction, and the performance of the sub-components, such kind of capabilities have not been achieved with a compact sensor package yet. To address this issue, this paper reports a new DMDSM sensor design. To enhance the material/thickness sensing capability by pulse-echo ultrasound, a novel ultrasound transmitter has been developed to provide wideband acoustic spectra. A new integration strategy has been adopted to accommodate all sensor components in a compact package. To verify our design, a prototype DMDSM sensor has been designed, fabricated and tested. The testing results show that the new DMDSM sensor can achieve similar ranging and better material/thickness sensing performance than the previously reported devices [25] [26]. More importantly, they can function well on OACTs, which makes it more practical for real applications in robotic grasping.

II. Sensor Design and Operation Principle

The schematic design of the new pulse-echo ultrasound and optoacoustic DMDSM sensor is shown in Fig. 2. A ring piezoelectric (lead zirconate titanate - PZT) transducer (with a center frequency of 1~2 MHz) is used as both transmitter and receiver. For pulse-echo ultrasound ranging, the ring transducer sends an ultrasound pulse, which is reflected and focused onto the target surface by a 90-degree parabolic mirror. The reflected or back-scattered echo signal travels along the reverse path and is received by the ring transducer. The ranging is performed based on the time delay between the pulse and echo signals. For optoacoustic ranging, a pulsed laser beam is shot through the center hole of the ring transducer and is reflected and focused onto the target surface to excite wideband optoacoustic signals. Part of the optoacoustic signal travels along the reverse path and is received by the ring transducer. The ranging is performed based on the time delay between the laser triggering and the received optoacoustic signal.

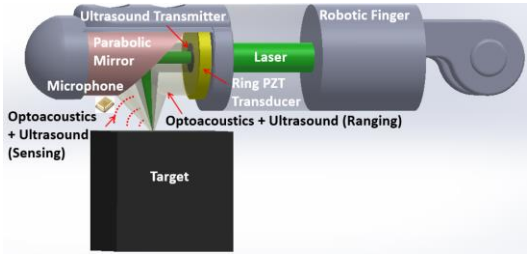

Figure 2. Schematic of the pulse-echo ultrasound and optoacoustic DMDSM sensor mounted onto a robotic finger.

For targets made of solid or layered materials with thicknesses of mm to cm, the lower-frequency components of the acoustic spectra (up to 10s of kHz) often carry more distinctive features about the material properties and sub-surface structures [27] [28] [29] [30]. Therefore, for optoacoustic material/thickness sensing, a wideband microphone (with an operation range of 0~10s of kHz) is used as the receiver to detect the low-frequency components of the (wideband) optoacoustic signal. However, due to lack of suitable ultrasound transmitters, this creates a challenge in the material/thickness sensing with pulse-echo ultrasound. This is because the microphone can only function as a receiver, while the ring PZT transducer operates at much higher frequencies. Conventional air-coupled transducers are typically narrow-band devices, and such bandwidth cannot be readily obtained with a single transducer. In addition, it is not feasible to accommodate multiple transducers in the (compact) sensor package.

As a key innovative feature in the DMDSM sensor design, a new optoacoustic wideband ultrasound transmitter has been developed to address this issue. The optoacoustic approach is adopted for its capability of wideband transmission. As shown in Fig. 3, the optoacoustic wideband ultrasound transmitter consists of a plastic frame with an array of through holes of the same diameter (except the central one), which are covered by a thin layer of laser absorptive polymer material. The other side of the frame is bonded with a shadow mask layer, such that only the free-standing polymer membranes can be effectively illuminated by the pulsed laser for sound generation. The ultrasound from the array of small-diameter polymer membranes merges into a wideband and planar wave, which is reflected and focused onto the target by the parabolic mirror. Laser-absorptive polymer material is selected because of its relatively low Young's modulus and high damping properties, which are more effective for wideband ultrasound transmission. The hole diameter and the distribution of the transmitter array are specially designed to provide a matching bandwidth with that of the microphone. The wideband ultrasound transmitter is located inside the inner hole of the ring PZT transducer, which forms a co-centered and co-axial arrangement (Fig. 2). Table I lists the associated sensor components and their specific functionalities for the DMDSM distance ranging and material sensing.

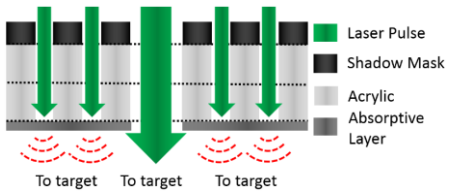

Figure 3. A diagram of the wideband ultrasound transmitter under pulsed laser illumination.

TABLE I. The Associated Sensor Components for DMDSM Distance Ranging and Material Sensing

	Pulse-echo Ultrasound	**Optoacoustics**
Distance Ranging	Ring transducer (transmitter and receiver)	Pulsed Laser (generator), Ring transducer (receiver)
Material Sensing	Wideband ultrasound (transmitter), Microphone (receiver)	Pulsed Laser (generator), Microphone (receiver)

III. Sensor Construction and Testing

Fig. 4 (a) shows the constructed prototype of the pulse-echo ultrasound and optoacoustic DMDSM sensor. It consists of a 3D-printed housing, a 90-degree parabolic mirror, a microphone with a reception bandwidth of 0~80

kHz, a home-made ring PZT transducer with 1-MHz resonance frequency, and a custom-made wideband ultrasound transmitter (Figs. 4 (b) and 4 (c)). A window tint film with 5% transmittance is used as the laser absorptive layer of the wideband ultrasound transmitter. The diameter of the central hole is 1.5 mm to allow the pulsed laser to pass through for conducting optoacoustic ranging and material sensing. The window tint film is bonded onto a laser-cut acrylic frame with an array of 28 through holes with a diameter of 0.5 mm, which also defines the size of the vibrating membrane for optoacoustic sound generation. The other side of the frame is covered with a thick layer of black tape as the shadow mask to prevent the direct illumination of the bonded portion of the window tint film.

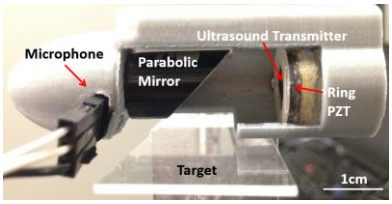

(a)

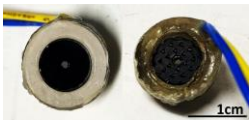

(b) (c)

Figure 4. Photographs of (a) the constructed prototype DMDSM sensor, (b) the wideband ultrasound transmitter inside the inner hole of the ring PZT transducer (front view on left and back view on right), and (c) the wideband ultrasound transmitter only (front view on left and back view on right).

To verify the acoustic performance of the wideband ultrasound transmitter, an ultrasound testing is conducted to characterize its transmission bandwidth (Fig. 5 (a)). A Q-switched 532-nm Nd:YAG pulsed laser is used as the light source with a repetition rate of 10 Hz, a pulse duration of 8 ns, and an average pulse energy of 20 mJ/pulse. The laser beam from the pulsed laser is firstly expanded by two lenses and then filtered by an iris. Based on the area ratio of the vibrating membranes and the whole illuminated region, the laser pulse energy deposition onto each membrane is estimated to be 60 μJ/pulse. To receive the optoacoustic signal, the microphone is fixed at 3 cm in front of the transmitter. A photo detector is used to detect the laser pulse and generate a trigger signal to synchronize the data acquisition. The received signals are amplified by the embedded preamplifier of an ultrasound pulser-receiver and recorded by an oscilloscope. A representative waveform and its frequency spectrum received by the microphone are shown in Figs. 5 (b) and 5 (c). The time-domain waveform consists of a series of pulses due to the multiple reflections between the transmitter and the microphone. The frequency spectrum indicates the transmitted bandwidth ranges from 0 to 90 kHz.

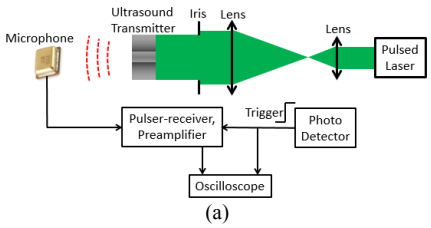

(a)

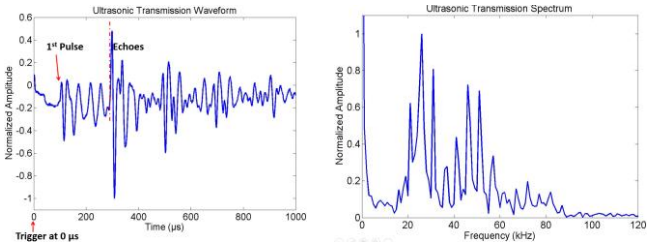

(b) (c)

Figure 5. (a) Diagram of the ultrasound testing setup to characterize the wideband ultrasound transmitter. (b) Representative waveform and (c) frequency spectrum of the ultrasound signal received by the microphone.

IV. Ranging Experiment and Results

A testing setup has been built to characterize the pulse-echo ultrasound and optoacoustic ranging and sensing performance of DMDSM sensor (Fig. 6). The same pulsed laser setup is used as the light source for optoacoustic excitation (Fig. 5 (a)). The central part of the laser beam passes through the wideband ultrasound transmitter and is incident onto the target for optoacoustic distance ranging and material sensing (Fig. 6 (b)). The outer part of the laser beam is incident onto the ultrasound transmitter to excite and send a wideband ultrasound pulse onto the target for pulse-echo ultrasound material sensing (Fig. 6 (c)). Driven by the pulser-receiver, the ring PZT transducer transmits an ultrasound pulse to the target and also receives the echo signal from the target for pulse-echo ultrasound distance ranging (Fig. 6 (d)). Both the laser and the transmitted ultrasound are reflected and focused by the parabolic mirror to improve the lateral resolution. The higher-frequency components of the excited optoacoustic signals and reflected ultrasound signals are received by the ring PZT transducer for distance ranging, while the lower-frequency ones are detected by the microphone for material sensing. For simultaneous DMDSM distance ranging and material sensing, a photo detector is used to detect the laser pulse and generate a trigger signal to synchronize the operations of the pulsed laser, the pulser-receiver and the oscilloscope. The received signals are amplified by the preamplifier embedded in the pulser-receiver, captured and recorded by the oscilloscope.

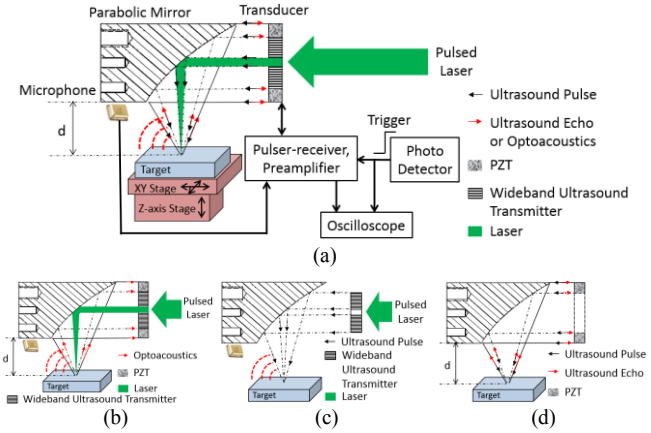

(a) (b) (c) (d)

Figure 6. Diagrams of (a) the general setup to characterize the pulse-echo ultrasound and optoacoustic ranging and sensing performance of the DMDSM sensor, (b) the sub-setup of optoacoustic distance ranging and material sensing, (c) the sub-setup of pulse-echo ultrasound material sensing, (d) the sub-setup of pulse-echo ultrasound distance ranging.

A. *Pulse-echo Ultrasound Distance Ranging*

For pulse-echo ultrasound distance ranging, a piece of 1-mm-thickness glass slide is used as the target [26]. The distance (d) between the parabolic mirror and the glass slide is decreased from 6.5 mm to 0 with a decrement of 0.5 mm. Fig. 7 (a) shows a representative pulse-echo ultrasound signal from the ring PZT transducer. The measured distance vs. the real distance (d) and their deviations are shown in Figs. 7 (b) and 7 (c), respectively. The deviation is smaller than 0.24 mm when the target is within the ultrasound focal zone where d is between 3.5 mm and 5.5 mm. The same setup is used to quantify the lateral resolution of the pulse-echo ultrasound, except that the glass slide target is replaced by a copper wire with a diameter around 0.7 mm. After repeating the linear scan at different distance (d) from 1.5 mm to 6.5 mm, the ultrasound lateral resolution is determined by the minimal acoustic focal diameter (Fig. 7 (d)), indicating the lateral resolution is around 1.04 mm at the focal length d = 4.5 mm. The measured depth of focus is around 2.0 mm where d is from 3.5 mm to 5.5 mm.

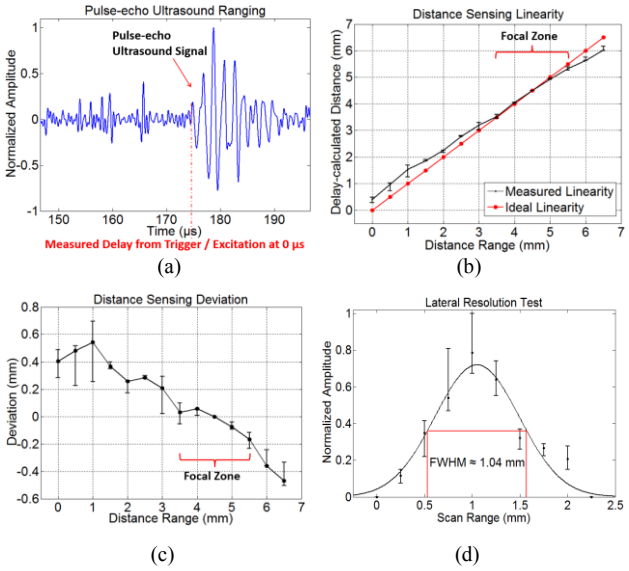

Figure 7. (a) Representative pulse-echo ultrasound signal, showing the measured delay from trigger / excitation. (b) Comparison between measured (in black) and real (in red) distances. (c) Deviation of the measured distance from the real distance. (d) Ultrasound lateral resolution 1.04 mm determined from the minimal acoustic focal diameter at d=4.5 mm.

B. *Optoacoustic Distance Ranging*

The optoacoustic distance ranging is characterized with a thin 0.1-mm copper wire as the target [25]. The distance (d) between the parabolic mirror and the target is decreased from 8 mm to 5 mm with a decrement of 0.5 mm. Fig. 8 (a) shows a representative optoacoustic signal received by the ring PZT transducer. The measured distance vs. the real distance (d) and their deviations are shown in Figs. 8 (b) and 8 (c), respectively. The deviation is smaller than 0.12 mm when the target is within the optoacoustic focal zone where d is between 5.5 mm and 6.5 mm. The same setup (Fig. 6) is used to quantify the optoacoustic lateral resolution, where the same copper wire is scanned laterally. After repeating the linear scan at different distance (d) from 5.0 mm to 8.0 mm, the optoacoustic lateral resolution is determined by the minimal optoacoustic focal diameter (Fig. 8 (d)), indicating the lateral resolution around 95 μm at the focal length d = 6.0 mm. The measured depth of focus is around 1.0 mm where d is from 5.5 mm to 6.5 mm.

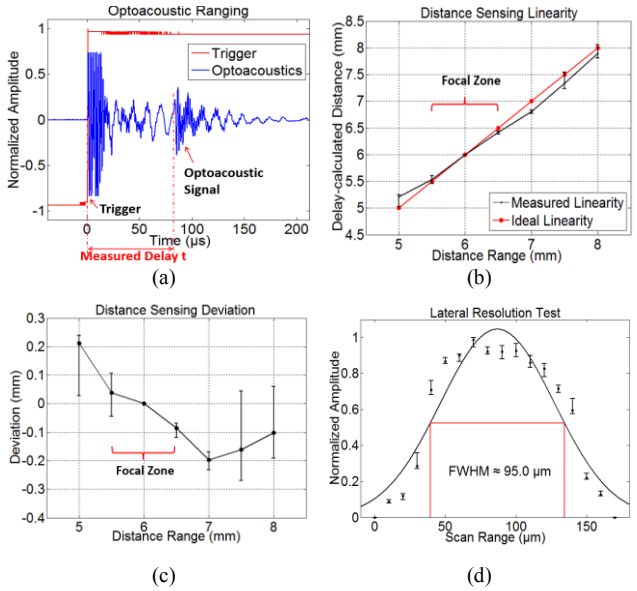

Figure 8. (a) Representative optoacoustic signal, showing the measured delay between "Trigger" and "Optoacoustic Signal". (b) Comparison between the measured (in black) and the real (in red) distances. (c) Deviation of the measured distance from the real distance. (d) Optoacoustic lateral resolution 95 μm determined from the minimal optoacoustic focal diameter at d = 6.0 mm.

V. Material Sensing Experiment and Results

A. *Data Acquisition and Classification*

For material sensing, the lower-frequency components of the excited optoacoustic and reflected ultrasound echo signals received by the microphone are used. Theoretically, the optoacoustic signals will arrive at the microphone earlier than the ultrasound echoes because of its shorter travel distance (e.g., from target to microphone vs. from transmitter to target and then microphone) (Fig. 6). However, due to their relatively long durations, these lower-frequency components would mix with each other when received by the same microphone. Depending on the optical and mechanical properties of the target, the received signals could mainly consist of either target-induced optoacoustic signal, or target-reflected ultrasound echo signal, or both. This kind of DMDSM signals is expected to provide more distinctive features for the material sensing. The material differentiation is performed with a Bag-of-SFA-Symbols (BOSS) classifier [31] [32]. The classifier is trained to identify the different materials, where the original data set is randomly divided into the training and testing data with 3:1 ratio without overlapping. The experimental data are transformed into BOSS histograms, serving as feature set for classification. After 50 random trials, the BOSS classifier gives the confusion matrix to show the accuracy of classification.

B. *Material/Thickness Differentiation*

To compare the performance of the new DMDSM sensor with that of the previous works [25] [26], the same group of targets, including steel, aluminum, acrylic, rubber, paper, and also aluminum sheets with different thickness have been used

for material/thickness differentiation. Unlike the previous experiments, no black ink is coated on the targets even with low optical absorption. The collected DMDSM acoustic spectra are shown in Figs. 9 and 10. The confusion matrices given by BOSS classifier indicate a 100% accuracy of the material differentiation and thickness classification (Fig. 11), which is even better than the accuracies of 87% - 97% and 94% - 100% obtained in previous works [25] [26].

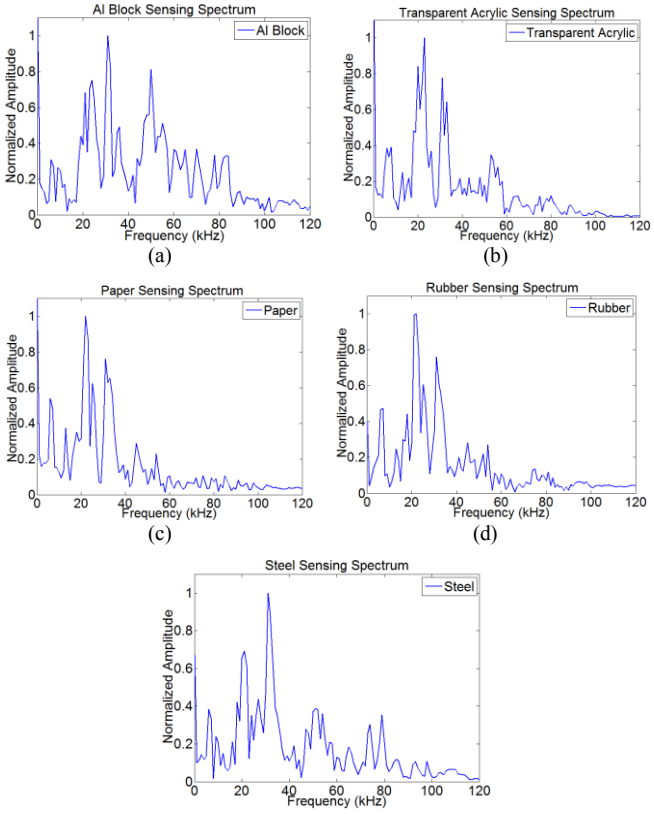

Figure 9. Representative DMDSM acoustic spectra from (a) aluminum block, (b) acrylic, (c) paper, (d) rubber, and (e) steel.

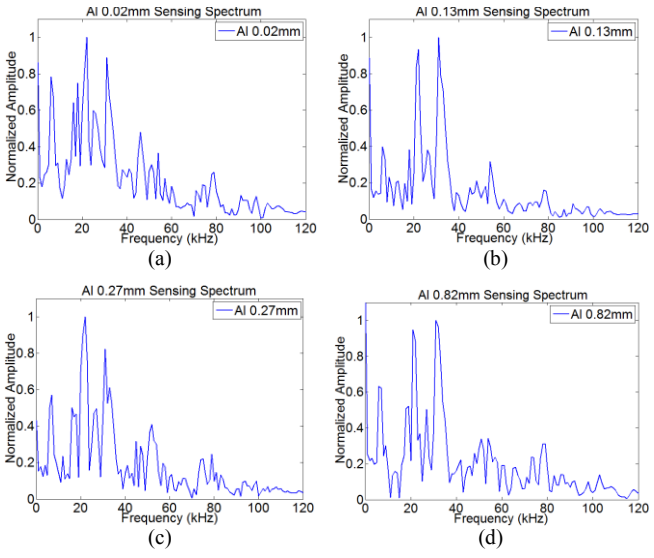

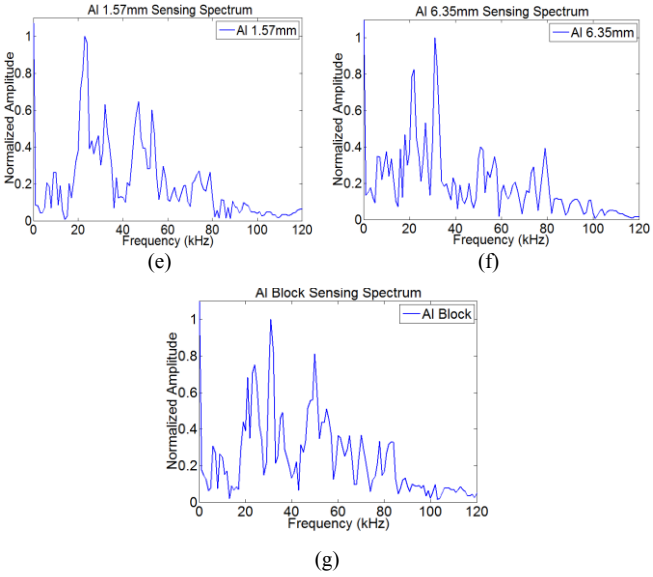

Figure 10. Representative DMDSM acoustic spectra from aluminum sheets with different thickness.

Figure 11. BOSS classifier averaged confusion matrix of (a) different materials and (b) aluminum sheets with different thickness.

C. Differentiation of Challenging Targets

To demonstrate the enhanced material sensing capabilities of the new DMDSM sensor, eight OACTs are tested (Fig. 12), including four optically-transparent targets of glass, acrylic, PET (polyethylene terephthalate), PDMS (polydimethylsiloxane) (Figs. 12 (a)-(d)) with low optoacoustic generation efficiency, and four dark thin/porous targets of fabric, foam, paper, window tint film (Figs. 12 (e)-(h)) with weak acoustic reflection. To compensate the target thickness difference, the height of Z-axis stage is adjusted until the target top is at the focus of the parabolic mirror (Fig. 6). The representative DMDSM acoustic spectra from the eight targets are shown in Fig. 13. BOSS classifier gives the confusion matrix showing an 100% accuracy for all the targets (Fig. 14). This result demonstrates the capability of differentiating OACTs with the new DMDSM sensor.

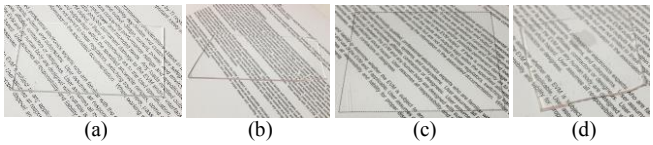

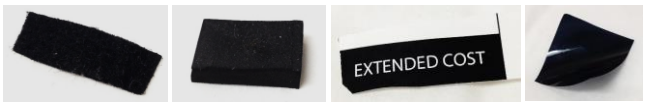

(e) (f) (g) (h)

Figure 12. Photos of the eight OACTs: (a)–(d) optically-transparent targets of glass, acrylic, PET (with contour marked by dash line), PDMS with thicknesses around 1.0 mm, 1.6 mm, 0.11 mm, and 1.5 mm separately, and (e)–(h) dark thin/porous targets of fabric, foam, paper, window tint film with thicknesses around 2 mm, 8 mm, 0.1 mm, 0.06 mm separately.

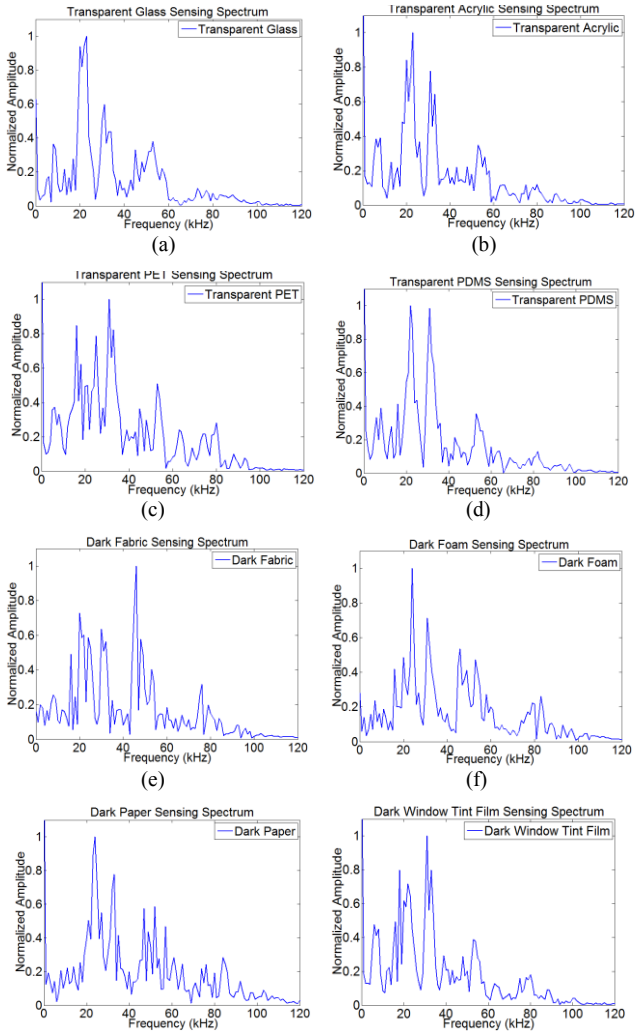

(a) (b) (c) (d) (e) (f) (g) (h)

Figure 13. Representative DMDSM acoustic spectra from (a)–(d) optically-transparent targets and (e)–(h) dark thin/porous targets.

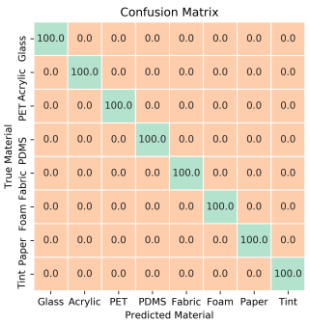

Figure 14. BOSS classifier averaged confusion matrix of the eight OACTs.

VI. Conclusion and Future Work

In this paper, we have demonstrated a fingertip mounted pulse-echo ultrasound and optoacoustic sensor for DMDSM near-distance ranging and material sensing in robotic grasping. The new DMDSM sensor is capable of differentiating not only conventional targets but also OACTs with high accuracy, which makes it more practical for real applications in robust and nimble robotic grasping. In the future, we plan to test more materials and sub-surface structures to optimize the ranging and sensing performance, and also integrate the sensor into robot fingers to develop perception algorithms to enable real time close-loop grasping.

Acknowledgment

The authors would like to thank for the inputs and feedback from Xiaoyu Duan.

References

[1] M. T. Mason, Mechanics of Robotic Manipulation, MIT press, 2001.

[2] M. Ciocarlie, K. Hsiao, E.G. Jones, S. Chitta, R.B. Rusu and I.A. Şucan, "Towards reliable grasping and manipulation in household environments," *Experimental Robotics,* pp. 241-252, Springer, Berlin, Heidelberg, 2014.

[3] K. Y. Goldberg, "Orienting Polygonal Parts Without Sensors," *Algorithmica,* vol. 10, no. 2-4, pp. 201-225, 1993.

[4] M. A. Erdmann and M. T. Mason, "An exploration of sensorless manipulation," *IEEE Journal on Robotics and Automation,* vol. 4, no. 4, pp. 369-379, 1988.

[5] C. E. Smith and N. P. Papanikolopoulos, "Vision-Guided Robotic Grasping: Issues and Experiments," *Proceedings of IEEE International Conference on Robotics and Automation,* vol. 4, pp. 3203-3208, 1996.

[6] A. Wehr and U. Lohr, "Airborne laser scanning—an introduction and overview," *ISPRS Journal of photogrammetry and remote sensing,* vol. 54, no. 2-3, pp. 68-82, 1999.

[7] Y. Lu, J. Lee, S. H. Yeh, H. M. Cheng, B. Chen and D. Song, "Sharing Heterogeneous Spatial Knowledge: Map Fusion between Asynchronous Monocular Vision and Lidar or Other Prior Inputs," *Robotics Research,* pp. 727-741, Springer, Cham, 2020.

[8] M. C. Amann, T. M. Bosch, M. Lescure, R. A. Myllylae and M. Rioux, "Laser ranging: a critical review of unusual techniques for distance measurement," *OptEn,* vol. 40, pp. 10-19, 2001.

[9] A. Stelzer, M. Jahn and S. Scheiblhofer, "Precise distance measurement with cooperative FMCW radar units," *2008 IEEE Radio and Wireless Symposium,* pp. 771-774, 2008.

[10] R. D. Howe, "Tactile sensing and control of robotic manipulation," *Advanced Robotics,* vol. 8, no. 3, pp. 245-261, 1993.

[11] J. M. Romano, K. Hsiao, G. Niemeyer, S. Chitta and K. J. Kuchenbecker, "Human-Inspired Robotic Grasp Control With Tactile Sensing," *IEEE Transactions on Robotics,* vol. 27, no. 6, pp. 1067-1079, 2011.

[12] Q. Xu, "Design and Development of a Novel Compliant Gripper With Integrated Position and Grasping/Interaction Force Sensing," *IEEE Transactions on Automation Science and Engineering,* vol. 14, no. 3, pp. 1415 - 1428, 2015.

[13] J. R. Smith, E. Garcia, R. Wistort and G. Krishnamoorthy, "Electric field imaging pretouch for robotic graspers," *2007 IEEE/RSJ International Conference on Intelligent Robots and Systems,* pp. 676-683, 2007.

[14] R. Wistort and J. R. Smith, "Electric field servoing for robotic manipulation," *In 2008 IEEE/RSJ International Conference on Intelligent Robots and Systems,* pp. 494-499, 2008, September.

[15] B. Mayton, L. LeGrand and J. R. Smith, "An electric field pretouch system for grasping and co-manipulation," *2010 IEEE International Conference on Robotics and Automation,* pp. 831-838, 2010.

[16] B. Mayton, E. Garcia, L. LeGrand and J. R. Smith, "Electric field pretouch: Towards mobile manipulation," *In RSS Workshop on Mobile Manipulation in Human Environments,* 2009, June.

[17] K. Hsiao, P. Nangeroni, M. Huber, A. Saxena and A. Y. Ng, "Reactive grasping using optical proximity sensors," *2009 IEEE International Conference on Robotics and Automation,* pp. 2098-2105, 2009.

[18] B. Yang, P. Lancaster and J. R. Smith, "Pre-touch sensing for sequential manipulation," *2017 IEEE International Conference on Robotics and Automation (ICRA),* pp. 5088-5095, 2017.

[19] H. Hasegawa, Y. Mizoguchi, K. Tadakuma, A. Ming, M. Ishikawa and M. Shimojo, "Development of intelligent robot hand using proximity, contact and slip sensing," *In 2010 IEEE International Conference on Robotics and Automation,* pp. 777-784, 2010, May.

[20] A. Maldonado, H. Alvarez and M. Beetz, "Improving robot manipulation through fingertip," *In 2012 IEEE/RSJ International Conference on Intelligent Robots and Systems,* pp. 2947-2954, 2012.

[21] L. Jiang and J. R. Smith, "A unified framework for grasping and shape acquisition via pretouch sensing," *In 2013 IEEE International Conference on Robotics and Automation,* pp. 999-1005, 2013, May.

[22] E. Guglielmelli, V. Genovese, P. Dario and G. Morana, "Avoiding obstacles by using a proximity us/ir sensitive skin," *In Proceedings of 1993 IEEE/RSJ International Conference on Intelligent Robots and Systems (IROS'93),* vol. 3, pp. 2207-2214, 1993, July.

[23] L. Jiang and J. R. Smith, "Seashell effect pretouch sensing for robotic grasping," *In 2012 IEEE International Conference on Robotics and Automation,* pp. 2851-2858, 2012, May.

[24] L. T. Jiang and J. R. Smith, "Pretouch sensing for manipulation," *In Robotics: Science and Systems (RSS) Workshop: Alternative Sensing Techniques for Robotic Perception,* 2012, July.

[25] C. Fang, D. Wang, D. Song and J. Zou, "Fingertip Non-Contact Optoacoustic Sensor for Near-Distance Ranging and Thickness Differentiation for Robotic Grasping," *2020 IEEE International Conference on Robotics and Automation (Accepted),* 2020.

[26] C. Fang, D. Wang, D. Song and J. Zou, "Toward Fingertip Non-Contact Material Recognition and Near-Distance Ranging for Robotic Grasping," *2019 IEEE International Conference on Robotics and Automation (ICRA),* pp. 4967-4974, 2019.

[27] I. P. Dunn and W. A. Davern, "Calculation of acoustic impedance of multi-layer absorbers," *Applied acoustics,* vol. 19, no. 5, pp. 321-334, 1986.

[28] M. E. Delany and E. N. Bazley, "Acoustical Properties of Fibrous Absorbent Materials," *Applied acoustics= Acoustique appliqu = Angewandte Akustik,* vol. 3, no. 2, pp. 105-116, 1970.

[29] M. I. Khan and G. J. Diebold, "The photoacoustic effect generated by laser irradiation of an isotropic solid cylinder," *Ultrasonics,* vol. 34, no. 1, pp. 19-24, 1996.

[30] R. D. Mindlin and H. Deresiewicz, "Thickness-shear and flexural vibrations of a circular disk," *Journal of applied physics,* vol. 25, no. 10, pp. 1329-1332, 1954.

[31] P. Schäfer, "The BOSS is concerned with time series classification in the presence of noise," *Data Mining and Knowledge Discovery,* vol. 29, no. 6, pp. 1505-1530, 2015.

[32] A. Bagnall, J. Lines, A. Bostrom, J. Large and E. Keogh, "The great time series classification bake off: a review and experimental evaluation of recent algorithmic advances," *Data Mining and Knowledge Discovery,* vol. 31, no. 3, pp. 606-660, 2017.